Applied Catalysis B: Environmental 158–159 (2014) 112–118

Contents lists available at ScienceDirect

Applied Catalysis B: Environmental

journal homepage: www.elsevier.com/locate/apcatb

Compressive strain as the main origin of enhanced oxygen reduction reaction activity for Pt electrocatalysts on chromium-doped titania support

Jun-Hyuk Kim [a], Seohyoung Chang [b], Yong-Tae Kim [a,*]

[a] School of Mechanical Engineering, Pusan National University, Busan 609-735, Republic of Korea
[b] Materials Science Division, Argonne National Laboratory, IL 60439, USA

ARTICLE INFO

Article history:
Received 28 November 2013
Received in revised form 29 March 2014
Accepted 3 April 2014
Available online 13 April 2014

Keywords:
Pt-based fuel cell electrocatalysts
Oxide supports
Charge transfer
Lattice strain
Oxygen reduction reaction

ABSTRACT

In this study, we have attempted to clarify the origin of the enhanced oxygen reduction reaction (ORR) activity of Pt on titania supports, which has been the subject of significant debate. To date, it has been claimed in several studies that the charge transfer from titania to Pt is the main origin of the enhanced ORR activity, while the theoretical adsorption model suggested that such charge transfer to Pt could lead to stronger OH adsorption and therefore a negative effect on ORR activity. We resolve this controversy by considering a lattice strain effect induced by the strong metal support interaction. EXAFS studies clearly show that a compressive strain leading to a lower *d*-band center is exerted on the Pt lattice on the titania-based supports. Hence, we strongly suggest that the main origin for the enhanced ORR activity is the compressive strain rather than the charge transfer.

1. Introduction

Because the oxygen reduction reaction (ORR) at the cathode has a significant overpotential in proton exchange membrane fuel cells (PEMFCs), it is essential to develop better electrocatalysts to enhance the ORR activity [1,2]. There have been several attempts to increase the ORR activity through, for instance, metal nanoparticle size or shape modification [3–5], metal alloying or dealloying [6–9], core–shell structure formation [10,11], or the deployment of oxide supports for the electrocatalyst to achieve a strong metal-support interaction [12] (SMSI). Among them, since the oxide supports can improve both the activity and durability through the SMSI and because their corrosion tolerance is higher than that of the conventional carbon supports, they have recently attracted intense interest from researchers in the electrocatalysis field. Most previous studies on oxide supports, however, have focused on only the durability enhancement due to their superior corrosion tolerance [13–16], while few papers have discussed the correlation between ORR activity and the SMSI. Theoretically, the correlation has been elucidated by the density functional theory (DFT) simulation performed by Linic et al. [17]. They suggested that when the electron charge transfer from a neighboring atom to Pt occurs, the chemical bond with surface hydroxyl (OH) becomes stronger, resulting in a negative effect on the ORR activity.

The conclusions of most of reports, however, conflict with this theoretical model. For example, Alonso-Vante et al. claimed that the Pt electron density was increased in the Pt/TiO_2 system based on lower observed shifts of the Pt 4*f* XPS signal, and they suggest that this density increase plays a key role in ORR activity enhancement [18]. Hwang et al. also suggested that the reason for the increased ORR activity was electron donation to Pt from an oxide such as $Ti_{0.7}Mo_{0.3}O_2$ [19] or TiO_2 [20], based on their analysis of the XANES white-line intensity. In other words, they concluded that the charge transfer is a major reason for the enhanced ORR activity. However, the theoretical model predicts that the charge transfer to Pt from the oxide supports will lead to a negative effect on the ORR activity. Hence, other factors should be considered in order to properly understand the origin of the ORR activity enhancement for Pt on titania supports. Even though both the lattice strain in Pt and the charge transfer are representative SMSI effects found in Pt on titania supports, no study investigating both effects simultaneously has been reported up to now.

Abbreviations: ORR, oxygen reduction reaction; PEMFCs, proton exchange membrane fuel cells; SMSI, strong metal-support interaction; DFT, density functional theory; XPS, X-ray photoelectron spectroscopy; XANES, X-ray absorption near edge structure; EXAFS, extended X-ray absorption fine structure; Cr-TiO_2, Cr-doped TiO_2 nanoparticles; TEM, transmission electron microscopy; XAS, X-ray absorption spectroscopy; DOS, density of states; CV, cyclic voltammetry; FWHM, full-width at half-maximum; ECSA, electrochemical surface area.

* Corresponding author. Tel.: +82 51 510 1012; fax: +82 51 514 0685.
E-mail addresses: yongtae@pusan.ac.kr, yongtaepnu@gmail.com (Y.-T. Kim).

http://dx.doi.org/10.1016/j.apcatb.2014.04.003
0926-3373/

In this study, we have investigated the lattice strain and the charge transfer simultaneously in order to resolve this controversy and to clarify the main origin of the enhanced ORR activity of Pt on titania supports. In particular, the doping of titania with Cr (Cr-TiO_2) enabled us to efficiently investigate such effects by increasing the electrical conductivity relative to that of bare titania. Pt/Cr-TiO_2 showed better ORR activity (higher specific activity at 0.9 V vs. RHE) than Pt/C. In order to identify the origin of the enhanced ORR activity, we discussed both the charge transfer based on the XPS analysis and the lattice strain based on EXAFS studies. Various high-resolution analysis techniques using a synchrotron beam revealed that, interestingly, the lattice strain effect is dominant in enhancing the ORR activity, in contrast with the previous discussion, where the charge transfer effect was considered to be the main factor involved in the increased ORR activity.

2. Experimental

2.1. Electrocatalyst synthesis

Cr-doped TiO_2 nanoparticles (Cr-TiO_2) were synthesized using a sol–gel and hydrothermal synthesis method. All the precursors were precisely measured to obtain a 5 mol% dopant ratio. Titanium isopropoxide (97%, Sigma Aldrich) and chromium nitrate (99%, Sigma Aldrich) were selected as precursors for the preparation of Cr-TiO_2 nanopowders, as reported in Kim and Han's paper [21]. Titanium isopropoxide was dispersed in acetic acid by stirring for 15 min, and then the solution was poured into an appropriate amount of distilled water with vigorous stirring for 1 h. Then, nitric acid was added to the solution, which was allowed to stand at 78 °C for 40 min, after which the temperature was continuously held for another 75 min with stirring. After this process, hydrothermal synthesis was conducted. Specifically, the solution mixed with distilled water was poured into an autoclave and the temperature was kept at 250 °C for 12 h. When the hydrothermal synthesis was finished, the solution was mixed with nitric acid and then stirred for 30 min. The prepared sample was fully filtered with distilled water then dried at 80 °C for 24 h. Then, the sample was heat-treated in the next step of the process. The sample was calcined to achieve crystallization at 500 °C for 4 h in an air atmosphere and then continuously calcined for dopant activation [22] at 300 °C for 2 h in an H_2 atmosphere. TiO_2 nanoparticles were synthesized with the same method for Cr-TiO_2 but without doping process.

Chloroplatinic acid hexahydrate (99.95%, Sigma Aldrich) was used as a precursor for the supported Pt samples. Pt nanoparticles were deposited on the surface of the support using sodium borohydride. First, the proper amount of Pt precursor was dissolved in distilled water. Then, the support material was dispersed in distilled water for 20 min using ultrasound and then vigorously mixed with the Pt precursor solution for 15 min. Next, the mixture of the Pt metal salt and support was reduced by the addition of the sodium borohydride solution. The precipitate was filtered and washed with distilled water then dried in oven at 80 °C for 24 h. For comparison, a Pt/C (Premetek, 20 wt% on Vulcan XC-72) electrocatalyst was also used.

2.2. Catalyst characterization

The amount of Pt was measured using an inductively coupled plasma optical emission spectrometer (ICP-OES, Ultima 2 CHR, KBSI PN317), and the existence of the TiO_2 phase was confirmed by an X-ray diffraction (XRD, Philips PANalytical) test in which Cu Kα radiation (λ = 1.5406 Å) was used. The morphology of the powders was observed using transmission electron microscopy (TEM, JEOL JEM-2011) in the KBSI Busan Center. The electrocatalyst nanopowders were dispersed in ethanol by sonication for the TEM specimen preparation. XPS (ESCALAB 250 Busan Center, KBSI) was used to observe the oxidation of Pt and to confirm the existence of the dopant. All XPS energy data were calibrated with the C 1*s* peak (284.6 eV). X-ray absorption spectroscopy (XAS) Pt L_3-edge data were recorded in the transmission mode at the Pohang accelerator laboratory (PAL) using the 7D XAFS beam line. The source of the beam was a bending magnet (1.4557 Tesla), and the monochromator was an Si (1 1 1) double crystal with an energy resolution ($\Delta\lambda/\lambda$) of 2×10^{-5} at 10 keV. The background absorption spectra were removed using the IFEFFIT software [23]. The *k*-space range was set to 3–13 $Å^{-1}$, and the EXAFS data were obtained by performing a Fourier transform on the *r*-space, which was set to 1.5–3 Å. All XAS spectra were calibrated with Pt foil. Calculations of the charge transfer and the electron density of states (DOS) were conducted using the CASTEP code. CASTEP is a DFT-based pseudopotential total-energy code. The occupied states of the electrons were calculated using the Perdew-Wang 1991 (PW91) functional based on the generalized gradient approximation (GGA) [24]. A plane-wave cutoff of 300 eV was used to ensure convergence in the geometry optimization and DOS calculation. A grid of $3 \times 3 \times 3$ *k*-points generated by the Monkhorst–Pack scheme was used in the calculations [25]. The structure of the unit cell lattice was optimized, and the charge transfer and DOS of Pt/Cr-TiO_2 system were calculated. The UV–visible absorption spectra of samples were measured with an UV spectrophotometer (650 UV–VIS, Ocean Optics). The carrier density, mobility and electric conductivity were measured with a Hall effect measurement system (HMS 5000, Ecopia) using the Van der Pauw method with sample powders pressed into pellets at a pressure of 10 tons [26]. Cyclic voltammetry (CV) and ORR polarization test were carried out to examine the electrochemical reaction occurring on the surface of the electrocatalyst. All electrochemical tests were carried out at room temperature and ambient pressure. All the samples were mixed with acetylene black carbon at a 5:2 mass ratio to improve the electrical conductivity within the thin electrodes using a slightly modified version of the procedure reported in Gasteiger and Shao's paper [27]. A three-electrode electrochemical cell on a potentiostat (Biologic VSP) was used. Well-dispersed electrocatalysts were deposited on a glassy carbon electrode that was used as a working electrode (5 mm in diameter). A platinum rod and an Ag/AgCl electrode were used as the counter and reference electrode, respectively. The proper amounts of distilled water, isopropanol, and Nafion solution were mixed with the electrocatalysts and dropped onto the working electrode surface to enhance the bond between the working electrode surface and the electrocatalyst.

3. Results and discussion

3.1. Morphology and structure

TEM micrographs for Pt/C and Pt/Cr-TiO_2 are given in Fig. 1. The Cr-TiO_2 nanoparticles are quite homogeneous, with sizes of about 10–15 nm. The supported Pt nanoparticles are also well-dispersed, with sizes of about 3–5 nm for the sample. In the Pt/C, the particle size is slightly smaller (about 2–4 nm) than in Pt/Cr-TiO_2. The XRD patterns of Pt/C, Pt/TiO_2, and Pt/Cr-TiO_2 are shown in Fig. 2. In these XRD patterns, the strongest diffraction peak is the (1 0 1) peak of the anatase phase at 25? Along with a few other (1 0 3), (0 0 4), (2 0 0), (1 0 5), and (2 1 1) peaks for the same phase. All peaks correspond well with the standard spectrum (JCPDS card No. 85-0439). For TiO_2 and Cr-TiO_2, only the anatase single phase

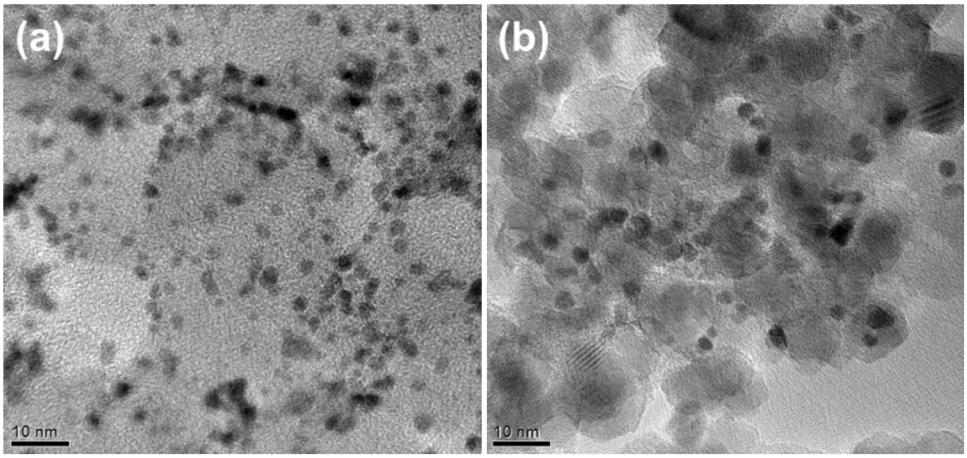

Fig. 1. TEM images of (a) Pt/C and (b) Pt/Cr-TiO_2.

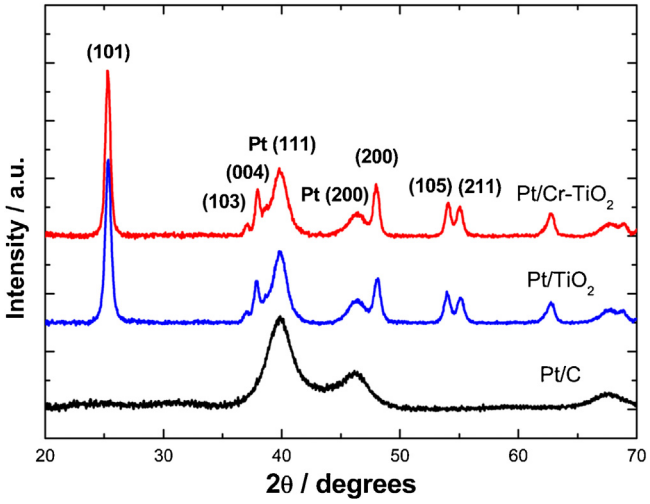

Fig. 2. XRD patterns of Pt/C, Pt/TiO_2 and Pt/Cr-TiO_2.

appeared, without any other phases such as the rutile and brookite phases. In general, the heat-treatment temperature is the dominant factor causing the phase transition of TiO_2 [25,26], although the characteristics of this phase can be affected by the type of dopant and its ratio [28–31]. In this study, since we synthesized the samples with a low heat-treatment temperature, no phase change occurred. As can be seen in Fig. 3a, the anatase phase (1 0 1) peak was shifted slightly in the negative angle direction when Cr was doped in the TiO_2, with a calculated position of 25.31° (Pt/Cr-TiO_2) instead of 25.34° (Pt/TiO_2). This can be explained by the different ionic radii of Ti^{4+} and Cr^{3+}. Since the ionic radius of Cr^{3+} (61.5 pm [32]) is larger than that of Ti^{4+}(60.5 pm [32]), lattice expansion might occur in TiO_2 when Cr is doped. The Pt peak was difficult to fit correctly because of overlaps with the anatase (1 0 3) and (0 0 4) peaks, but no significant peak shift was found in XRD spectrum, as shown in Fig. 3b. In order to analyze the fine structure with a higher resolution, we carried out EXAFS studies with the synchrotron beam, the details of which are discussed later in this paper.

The average particle sizes were calculated from the full-width at half-maximum (FWHM) using Scherrer's equation:

$$d = \frac{k\lambda}{\beta \cos\theta} \quad (1)$$

where d is the average particle size (Å), k is the shape-sensitive coefficient (0.9), λ is the wavelength (1.5490 Å), β is the FWHM (in radians) of the peak, and θ is the angle at the position of the peak maximum (in radians). The average particle size of the Cr-TiO_2 calculated from the anatase (1 0 1) diffraction peak was about 15 nm. In the same way, the particle size based on the Pt (1 1 1)

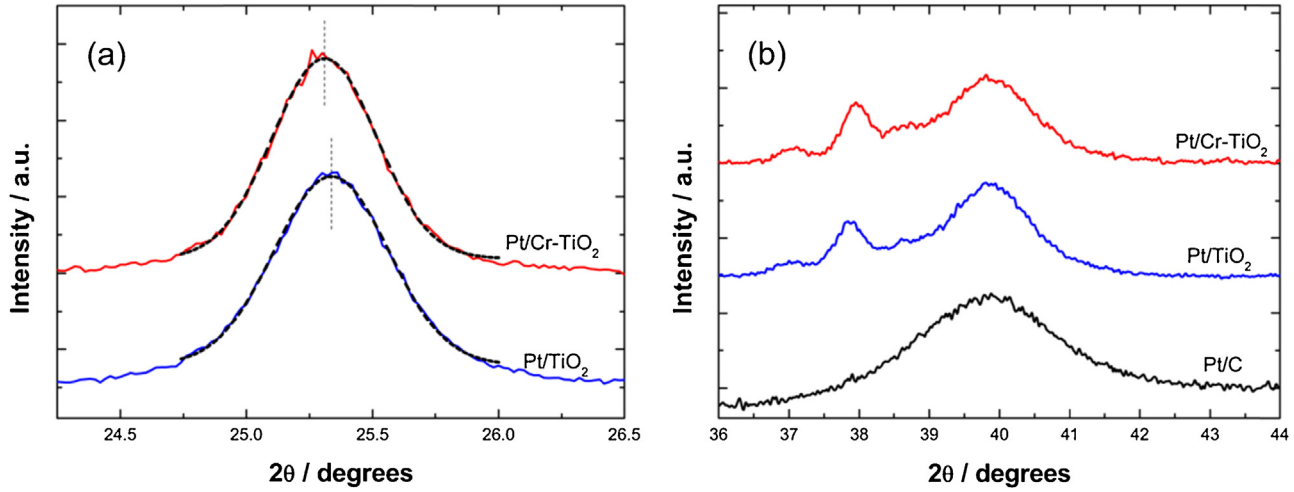

Fig. 3. Magnified (a) TiO_2 anatase (1 0 1) peaks for Pt/TiO_2 and Pt/Cr-TiO_2 and (b) Pt (1 1 1) peaks for Pt/C, Pt/TiO_2, and Pt/Cr-TiO_2. Peak fits are represented with the black-dashed line.

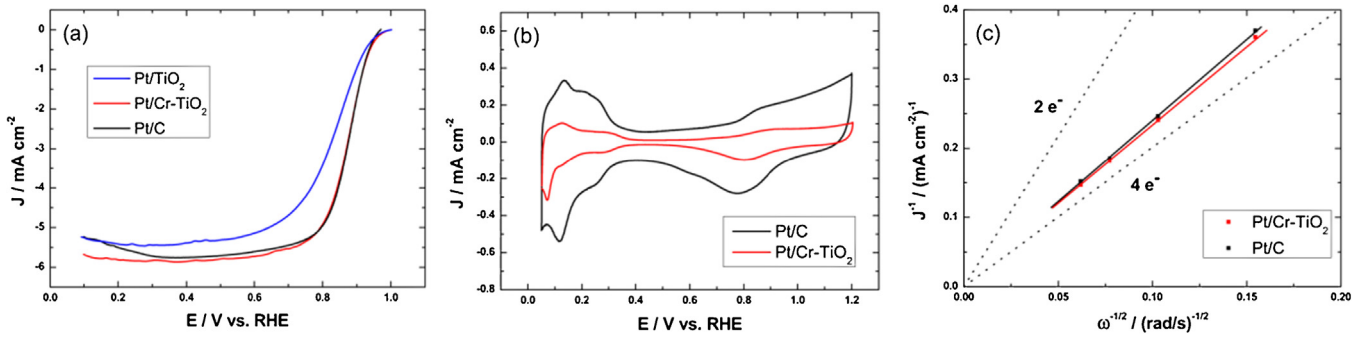

Fig. 4. (a) Comparison of the ORR activity of Pt/C, Pt/TiO_2, and Pt/Cr-TiO_2 at 1600 rpm. (b) CV curves for Pt/C and Pt/Cr-TiO_2. (c) Koutecky–Levich plots for the ORR at 0.8 V vs. RHE for Pt/C and Pt/Cr-TiO_2. All electrochemical tests were *I–R* corrected and oxygen environmental electrochemical tests were also corrected with double-layer capacitance.

peak was found to be about 4 nm for Pt/C and 5 nm for Pt/Cr-TiO_2. All the calculated particle sizes are in good agreement with the values obtained from the TEM results.

3.2. Electrochemical activity

ORR activity curves for Pt/C, Pt/TiO_2, and Pt/Cr-TiO_2 are given in Fig. 4a. There was no significant activity difference between Pt/C and Pt/Cr-TiO_2, while Pt/TiO_2 showed decreased ORR activity in the mixed kinetics- and diffusion-controlled region. A clear trend was apparent in the half-wave potential, as shown in Fig. 5a, with values of 0.830 V for Pt/TiO_2, 0.871 V for Pt/Cr-TiO_2, and 0.874 V for Pt/TiO_2. Since the electrical conductivity is an important factor in the optimization of the activity in the mixed kinetics- and diffusion-controlled region, the ORR activity of the Pt/Cr-TiO_2 increased more than that of Pt/TiO_2, because the electrical conductivity was markedly enhanced by the Cr doping. In order to exactly understand the main factors affecting the ORR kinetics, the electrical conductivity must be high enough to avoid any misleading ohmic loss. For this reason, no further investigation was performed for Pt/TiO_2, which had insufficient conductivity.

The specific activities for the samples were determined by calculating the electrochemical surface area (ECSA) based on cyclic voltammograms, as shown in Fig. 4b. ECSA can be calculated using the equation [33]

$$\mathrm{ECSA} = \frac{Q_H}{L \times q_H} \tag{2}$$

where L is the catalyst loading ($\mu g/cm^2$) on the working electrode; Q_H is the charge for the hydrogen adsorption (mC/cm^2), calculated as the mean value of the amounts of charge exchanged during the electroadsorption and electrodesorption of H_2 on the catalyst sites after the double-layer correction [34]; and q_H is the charge required to oxidize a monolayer of H_2 on Pt (0.21 mC/cm^2) [35].

The ECSA of the Pt/C was calculated as 61 m^2/g_{Pt}, which is consistent with the reported values of 66 m^2/g_{Pt} [1] and 65 m^2/g_{Pt} [36] within the margin of the measurement error, which is mainly caused by the variation in the film coating. The ECSA for the Pt/Cr-TiO_2 was also calculated as 18 m^2/g_{Pt}, which is much lower than that of the Pt/C. The specific activity based on the ECSA can be obtained as shown in Fig. 5b. The specific activities of the samples were calculated as 272 $\mu A/cm^2$ for Pt/TiO_2, 462 $\mu A/cm^2$ for Pt/Cr-TiO_2 and 141 $\mu A/cm^2$ for Pt/C. It is interesting to note that specific activity of the Pt/Cr-TiO_2 was nearly 3 times higher than that of the Pt/C. Although the ECSA of the Pt/Cr-TiO_2 was similar to the values (13 m^2/g_{Pt} [20 wt% Pt/VC] and 19 m^2/g_{Pt} [20 wt% Pt/VC]) by Ticianelli et al., the specific activity was higher than those reported study (210 $\mu A/cm^2$ and 170 $\mu A/cm^2$) [1,37]. It is inferred that size effect on the Pt/Cr-TiO_2 may influence the activity, however, it would not be the main reason. We suggest that SMSI could much affect the activity with consideration of the result that Pt/TiO_2 based support has lower ECSA than that of Pt/C [15,38–40]. As shown in Fig. 4c, the current densities measured at a constant potential were used to produce a Koutecky–Levich plot [41], which shows the inverse current density (J^{-1}) as a function of the inverse square root of the rotation rate ($\omega^{-1/2}$) and indicates first-order kinetics with respect to molecular oxygen. The Koutecky–Levich equation is written as

$$\frac{1}{j} = \frac{1}{j_k} + \frac{1}{j_d} = \frac{1}{j_k} + \frac{1}{B\omega^{1/2}} \tag{3}$$

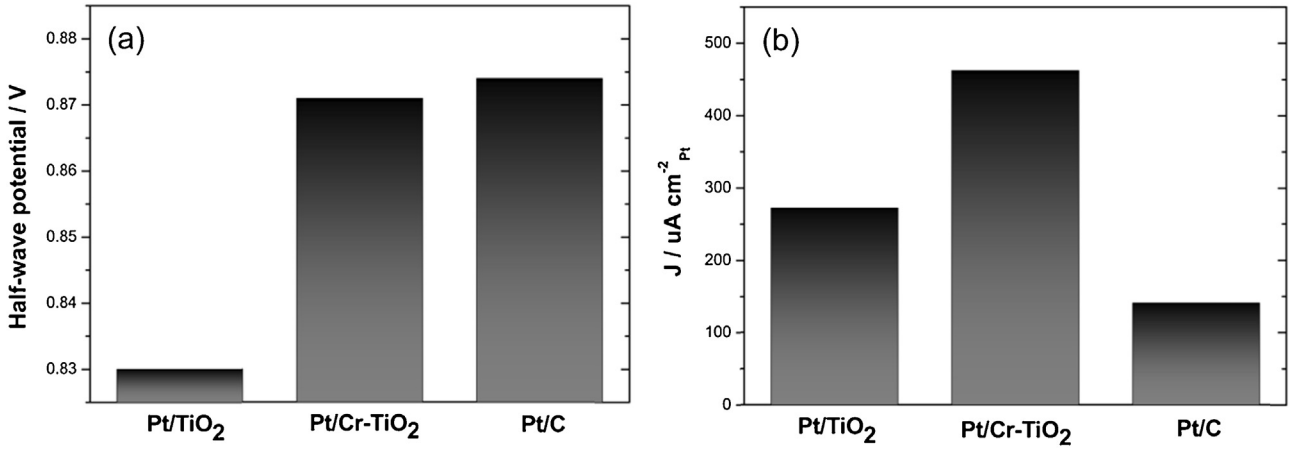

Fig. 5. (a) Half-wave potentials for Pt/TiO_2, Pt/Cr-TiO_2, and Pt/C. (b) Specific activities for Pt/C, Pt/TiO_2 and Pt/Cr-TiO_2 at 0.9 V.

Table 1
Distribution of Pt species and relative intensities that are observed from the XPS for the Pt/C and Pt/Cr-TiO_2.

Samples		Binding energy of Pt $4f_{7/2}$ (eV)	Relative intensity (%)
Pt/C	Pt^0	71.3	76.4
	Pt^{2+}	72.5	18.8
Pt/Cr-TiO_2	Pt^0	71.1	80.7
	Pt^{2+}	72.5	16.0

in which

$$B = \frac{0.62nFAC_{O_2}D_{O_2}^{2/3}}{\eta^{1/6}} \quad (4)$$

where j is the experimentally obtained current, j_k is the kinetic current, j_d is the diffusion-limited current, n is the number of electrons transferred, F is the Faraday constant ($F = 96485.3399$ C/mol), A is the geometric area of the electrode ($A = 0.19625\ cm^2$), C_{O_2} is the O_2 concentration in the electrolyte ($C_{O_2} = 1.26 \times 10^{-3}$ mol/L), D_{O_2} is the diffusion coefficient of O_2 in $HClO_4$ solution ($D_{O_2} = 1.93 \times 10^{-5}\ cm^2/s$), and η is the viscosity of the electrolyte ($\eta = 1.009 \times 10^{-2}\ cm^2/s$). The slope of the lines (j^{-1} versus $\omega^{-1/2}$) is $1/B$. The slope was calculated by linear fitting, and the n values were obtained as nearly 4. Specifically, the value of Pt/C was 3.9, and that of Pt/Cr-TiO_2 was 3.8.

Up to this point, we have measured the outstanding characteristics of the Pt/Cr-TiO_2 with electrochemical tests. However the question of where these characteristics come from remains. To explain this, we next focus on the competitive effects of charge transfer and lattice strain.

3.3. Charge transfer effect

We first focus on the effect of the ligand through charge transfer, which has been considered the main origin of the enhanced ORR activity up to now. When the metal surface interacts with adjacent material, charge transfer is induced by the difference in the electronic environment [42–45], which is in general referred to as the ligand effect. Markovic et al. reported the variation in the adsorption strength between surface atoms and adsorbate species due to charge transfer for Pt(1 1 1) and Pt_3Ni(1 1 1) polycrystals [43]. In addition, Tang and Henkelman claimed that charge redistribution plays an important role in the modification of chemical properties specifically for nanoparticle systems [46].

In this study, we analyzed the Pt 4*f* XPS spectra for Pt/C and Pt/Cr-TiO_2 to evaluate the ligand effect. The Pt 4*f* XPS core levels of the Pt/C and Pt/Cr-TiO_2 are shown in Fig. 6. The proportion of fully reduced Pt was much higher in the Pt/Cr-TiO_2, as shown in Table 1. In other words, Pt/Cr-TiO_2 has an electron-rich phase on its surface. This is in good agreement with the results found in the literature [19,40]; the electron charge transfer is higher in Pt/oxide than in Pt/C. This charge transfer can be explained in terms of Schottky theory [47]. Because the work function of Pt (Φ_{Pt}, W.F.) is higher than that of TiO_2, charge is transferred from TiO_2 to Pt at the interface. Moreover, since Cr-TiO_2 is an n-type doping system, with a donor level near the edge of the conduction band, the Fermi level of TiO_2 is shifted upward. Therefore $\Phi_{Cr\text{-}TiO_2}$ becomes lower, and the Schottky barrier is higher, increasing the charge transfer.

To obtain further insight into the effects of the charge transfer and its effect on the ORR activity, DFT calculations were performed, with the results shown in Table 2. The TiO_2 anatase (1 0 1) model was used as the structure of the support for the nanoclustered Pt. Ti atoms were replaced with Cr atoms in a 5% ratio for the Cr-TiO_2 structure. It was found that most charge transfer was to the *sp*-band rather than to the *d*-band.

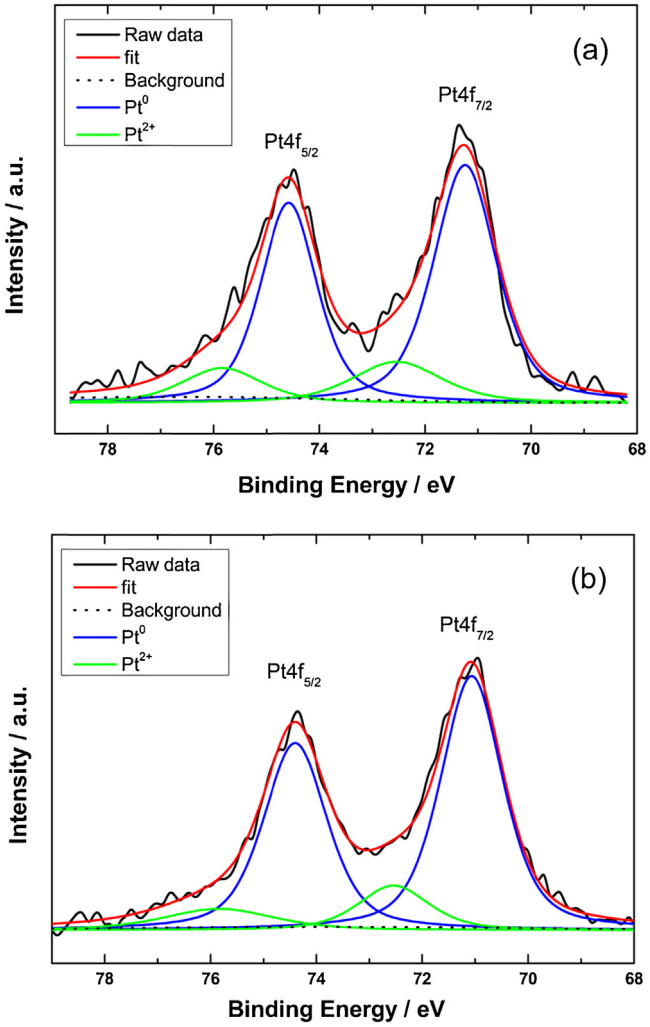

Fig. 6. Pt 4*f* XPS spectra and deconvoluted curves of (a) Pt/C and (b) Pt/Cr-TiO_2.

According to the study by Norskov and Chen et al., the correlation between the electron charge transfer and the changes in *d*-band electron filling is lower than 2%. Therefore, charge transfer to the *d*-band can be considered negligible [48]. When charge transfer is induced by the difference in electronegativity between Pt and the neighboring atom, the filling of the *sp*-band of Pt changes. In this environment, the Pt *sp*-band interacts with the OH adsorbate strengthening the bond governed by the Pt–OH distance [49]. Our calculated result, in agreement with the previous literature, clearly shows that the increase in the *sp*-band population due to charge transfer negatively affects the ORR activity.

3.4. Lattice strain effect

Until now, there has been little discussion in the literature on the strain effect in metal-oxide systems, although strain effect is another key factor affecting catalytic activity. To investigate this effect, EXAFS spectra of Pt/C and Pt/Cr-TiO_2 were obtained near the Pt L_3 edge (11,564 eV) and were processed by Fourier transformation, as depicted in Fig. 7. Strong peaks in regard to Pt–O and Pt–Pt 1NN were observed from $R = 1.6$ to 3.2 Å. The Pt atomic distance was determined by fitting the scattering path, Pt–O and Pt–Pt 1NN peaks, in *r*-space. The result is shown in the inset in Fig. 7. The Pt–Pt atomic distances in Pt/C and Pt/Cr-TiO_2 were calculated as 2.770 Å (±0.001) and 2.748 Å (±0.002), respectively. The data clearly show a lattice contraction in Pt/Cr-TiO_2 as a result of SMSI.

Table 2
Charge transfer for Pt/Cr-TiO_2. The values in round brackets represent the Pt charge 9 distribution without Cr-TiO_2.

Atom/orbital	*s*	*p*	*d*	*f*	Charge
Cr	2.290	6.280	4.490	0	0.940
O	1.862	4.787	0	0	−0.647
Ti	2.259	6.278	2.239	0	1.226
Pt	1.078 (0.730)	0.228 (0.560)	8.934 (8.710)	0	−0.238 (0)

It has been reported that the metal-adsorbate bond strength changes as a result of *d*-band center shifts due to strain variation in the metal structure. Such changes finally lead to changes in the adsorption strength [42,50,51], which is one of the critical factors affecting the ORR. Norskov et al. reported that the strain effect induces changes in the metal *d*-band by modifying the shape of the electron population [52]. Strasser et al. controlled the adsorption strength of oxygenated (O) species by inducing compressive strain with Pt (less reactive) and Cu (very reactive) in a core–shell system [42].

Furthermore, several researchers focused on the correlation between the adsorption strength and the ORR activity. Adzic et al. presented the volcano curve correlation between the *d*-band center position and the ORR activity and found that Pt needs to have lower *d*-band center position to achieve the best catalytic activity [53]. Norskov et al. revealed the correlation between the O species adsorption binding energy and the *d*-band center position [54] and also showed that the *d*-band center position shifts in response to tensile or compressive strain in Pt and Pt alloy systems [48]. For instance, under tensile strain, the overlap of the *d*-band decreases and becomes sharp, which results in upshifting of the *d*-band center. Finally, the adsorption strength of the O species increases. Under compressive strain, however, the effect is the opposite: the overlap increases, the shape of *d*-band broadens, and the *d*-band center is downshifted. In conclusion, compressive strain induces a downshift in the *d*-band center, pulling antibonding states further below the Fermi level and increasing Pauli repulsion [42]. This gives rise to weaker bonding with the O adsorbate, resulting in an increase in ORR activity.

We checked the Pt *d*-band electron density with DFT modeling, as shown in Fig. 8. The spectra are presented relative to the Fermi level at zero energy, and the *d*-band center was obtained by calculating the DOS below the Fermi level. The result shows that *d*-band was lower in Pt/Cr-TiO_2 than in Pt/C owing to the compressive strain. This is in good agreement with the results given in the above reports that the *d*-band broadens and downshifts relative to the Fermi level when compressive strain is introduced. That is to say, compressive strain in the Pt in Pt/Cr-TiO_2 brought about the downshift of the *d*-band center, and therefore the bond with O species became weak, resulting in enhancement of the ORR activity.

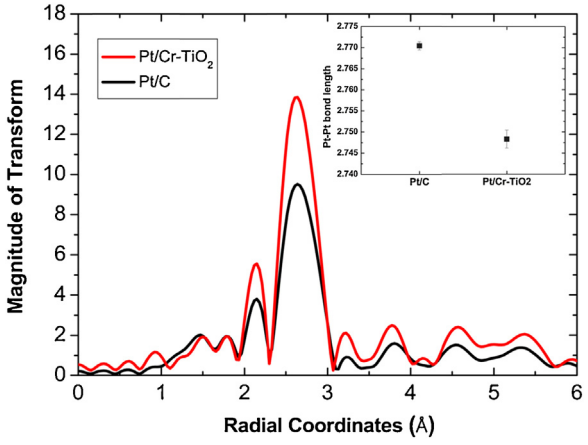

Fig. 7. Fourier transform magnitude spectra of the Pt L_3 edge for Pt/C and Pt/Cr-TiO_2.

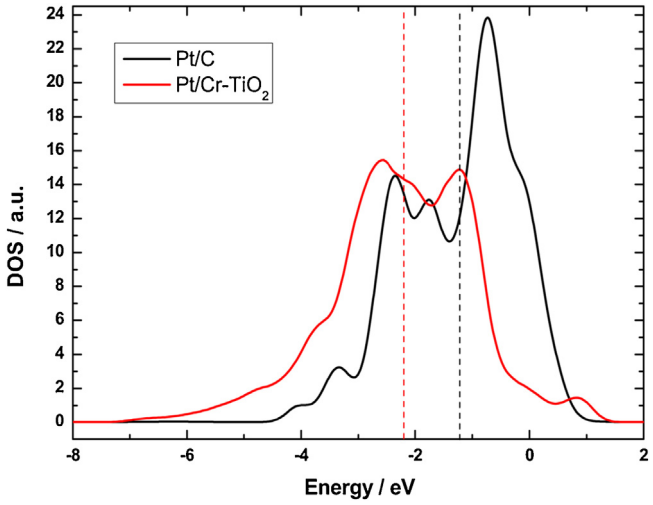

Fig. 8. Calculated *d*-band electron density for Pt/C and Pt/Cr-TiO_2. Dashed lines represent the *d*-band center position.

4. Conclusions

In this study, we discussed whether the main origin of the enhanced ORR activity of Pt/Cr-TiO_2 is strain or a ligand effect. Cr-TiO_2 was chosen to eliminate misleading side effects due to the low electrical conductivity of TiO_2. The ligand effect was confirmed by XPS, which showed that charge transfer from Cr-TiO_2 to Pt occurs, and it was concluded that the ligand effect makes the bond with OH adsorbate stronger, reducing the ORR activity. In addition, the strain effect was explained using the EXAFS technique. The Pt lattice in Pt/Cr-TiO_2 was confirmed to be in a strained state. This implies that the *d*-band center was downshifted, weakening the bond strength with the O adsorbate. This strain plays key roles in enhancing the ORR activity and is more dominant than the ligand effect.

Acknowledgement

This work was supported by a National Research Foundation of Korea Grant funded by the Korean Government (NRF-2012R1A1A2007624, NRF-2012K2A1A2032856, NRF-2012-M1A2A2-029543 and KCRC-2013M1A8A1040703).

Appendix A. Supplementary data

Supplementary data associated with this article can be found, in the online version, at http://dx.doi.org/10.1016/j.apcatb.2014.04.003.

References

[1] H.A. Gasteiger, S.S. Kocha, B. Sompalli, F.T. Wagner, Appl. Catal. B: Environ. 56 (2005) 9.

[2] P.J. Ferreira, G.J. la O', Y. Shao-Horn, D. Morgan, R. Makharia, S. Kocha, H.A. Gasteiger, J. Electrochem. Soc. 152 (2005) A2256.
[3] F.J. Perez-Alonso, D.N. McCarthy, A. Nierhoff, P. Hernandez-Fernandez, C. Strebel, I.E.L. Stephens, J.H. Nielsen, I. Chorkendorff, Angew. Chem. Int. Ed. 51 (2012) 4641.
[4] W. Sheng, S. Chen, E. Vescovo, Y. Shao-Horn, J. Electrochem. Soc. 159 (2012) B96.
[5] G.A. Tritsaris, J. Greeley, J. Rossmeisl, J.K. Norskov, Catal. Lett. 141 (2011) 909.
[6] C. Wang, M.F. Chi, D.G. Li, D. Strmcnik, D. van der Vliett, G.F. Wang, V. Komanicky, K.C. Chang, A.P. Paulikas, D. Tripkovic, J. Pearson, K.L. More, N.M. Markovic, V.R. Stamenkovic, J. Am. Chem. Soc. 133 (2011) 14396.
[7] N.M. Marković, T.J. Schmidt, V. Stamenković, P.N. Ross, Fuel Cells 1 (2001) 105.
[8] I.E.L. Stephens, A.S. Bondarenko, F.J. Perez-Alonso, F. Calle-Vallejo, L. Bech, T.P. Johansson, A.K. Jepsen, R. Frydendal, B.P. Knudsen, J. Rossmeisl, I. Chorkendorff, J. Am. Chem. Soc. 133 (2011) 5485.
[9] A.U. Nilekar, Y. Xu, J.L. Zhang, M.B. Vukmirovic, K. Sasaki, R.R. Adzic, M. Mavrikakis, Top. Catal. 46 (2007) 276.
[10] D. Wang, H.L. Xin, Y. Yu, H. Wang, E. Rus, D.A. Muller, H.D. Abruña, J. Am. Chem. Soc. 132 (2010) 17664.
[11] D.S. Kim, J.H. Kim, I.K. Jeong, J.K. Choi, Y.T. Kim, J. Catal. 290 (2012) 65.
[12] S.J. Tauster, S.C. Fung, R.T.K. Baker, J.A. Horsley, Science 211 (1981) 1121.
[13] D.-S. Kim, E.F.A. Zeid, Y.-T. Kim, Electrochim. Acta 55 (2010) 3628.
[14] S.Y. Huang, P. Ganesan, S. Park, B.N. Popov, J. Am. Chem. Soc. 131 (2009) 13898.
[15] C.V. Subban, Q. Zhou, A. Hu, T.E. Moylan, F.T. Wagner, F.J. DiSalvo, J. Am. Chem. Soc. 132 (2010) 17531.
[16] S.V. Selvaganesh, G. Selvarani, P. Sridhar, S. Pitchumani, A.K. Shukla, J. Electrochem. Soc. 157 (2010) B1000.
[17] H. Xin, A. Holewinski, N. Schweitzer, E. Nikolla, S. Linic, Top. Catal. 55 (2012) 376.
[18] A. Lewera, L. Timperman, A. Roguska, N. Alonso-Vante, J. Phys. Chem. C 115 (2011) 20153.
[19] T.T.H. Van, C.J. Pan, J. Rick, W.N. Su, B.J. Hwang, J. Am. Chem. Soc. 133 (2011) 11716.
[20] N.G. Akalework, C.J. Pan, W.N. Su, J. Rick, M.C. Tsai, J.F. Lee, J.M. Lin, L.D. Tsai, B.J. Hwang, J. Mater. Chem. 22 (2012) 20977.
[21] C. Kim, K.S. Kim, H.Y. Kim, Y.S. Han, J. Mater. Chem. 18 (2008) 5809.
[22] K.W. Park, K.S. Seol, Electrochem. Commun. 9 (2007) 2256.
[23] B. Ravel, M. Newville, J. Synch. Radiat. 12 (2005) 537.
[24] J.P. Perdew, J.A. Chevary, S.H. Vosko, K.A. Jackson, M.R. Pederson, D.J. Singh, C. Fiolhais, Phys. Rev. B 46 (1992) 6671.
[25] H.J. Monkhorst, J.D. Pack, Phys. Rev. B 13 (1976) 5188.
[26] H. Song, S.W. Yun, H.H. Chun, M.G. Kim, K.Y. Chung, H.S. Kim, B.W. Cho, Y.T. Kim, Energy Environ. Sci. 5 (2012) 9903.
[27] J. Suntivich, H.A. Gasteiger, N. Yabuuchi, Y. Shao-Horn, J. Electrochem. Soc. 157 (2010) B1263.
[28] M.A. Barakat, G. Hayes, S.I. Shah, J. Nanosci. Nanotechnol. 5 (2005) 759.
[29] B. Choudhury, A. Choudhury, Mater. Chem. Phys. 132 (2012) 1112.
[30] A.M. Ruiz, G. Dezanneau, J. Arbiol, A. Cornet, J.R. Morante, Chem. Mater. 16 (2004) 862.
[31] M.A. Gillispie, M.F.A.M. van Hest, M.S. Dabney, J.D. Perkins, D.S. Ginley, J. Mater. Res. 22 (2007) 2832.
[32] R.D. Shannon, C.T. Prewitt, Acta Crystallogr. B 25 (1969) 925.
[33] A. Pozio, M. De Francesco, A. Cemmi, F. Cardellini, L. Giorgi, J. Power Sources 105 (2002) 13.
[34] T.J. Schmidt, H.A. Gasteiger, G.D. Stäb, P.M. Urban, D.M. Kolb, R.J. Behm, J. Electrochem. Soc. 145 (1998) 2354.
[35] J. Perez, E.R. Gonzalez, E.A. Ticianelli, Electrochim. Acta 44 (1998) 1329.
[36] U.A. Paulus, A. Wokaun, G.G. Scherer, T.J. Schmidt, V. Stamenkovic, N.M. Markovic, P.N. Ross, Electrochim. Acta 47 (2002) 3787.
[37] E.A. Ticianelli, C.R. Derouin, S. Srinivasan, J. Electroanal. Chem. Interfacial Electrochem. 251 (1988) 275.
[38] S. Sun, G. Zhang, X. Sun, M. Cai, M. Ruthkosky, J. Nanotechnol. (2012) 8.
[39] N.R. Elezović, B.M. Babić, L. Gajić-Krstajić, V. Radmilović, N.V. Krstajić, L.J. Vračar, J. Power Sources 195 (2010) 3961.
[40] S. von Kraemer, J. Wikander, G. Lindbergh, A. Lundblad, A.E.C. Palmqvist, J. Power Sources 180 (2008) 185.
[41] M.H. Shao, T. Huang, P. Liu, J. Zhang, K. Sasaki, M.B. Vukmirovic, R.R. Adzic, Langmuir 22 (2006) 10409.
[42] P. Strasser, S. Koh, T. Anniyev, J. Greeley, K. More, C. Yu, Z. Liu, S. Kaya, D. Nordlund, H. Ogasawara, M.F. Toney, A. Nilsson, Nat. Chem. 2 (2010) 454.
[43] V.R. Stamenkovic, B. Fowler, B.S. Mun, G. Wang, P.N. Ross, C.A. Lucas, N.M. Marković, Science 315 (2007) 493.
[44] P. Liu, J.K. Norskov, Phys. Chem. Chem. Phys. 3 (2001) 3814.
[45] J.A. Rodriguez, D.W. Goodman, Science 257 (1992) 897.
[46] W.J. Tang, G. Henkelman, J. Chem. Phys. 130 (2009).
[47] N. Yamamoto, S. Tonomura, H. Tsubomura, J. Electrochem. Soc. 129 (1982) 444.
[48] J.R. Kitchin, J.K. Nørskov, M.A. Barteau, J.G. Chen, Phys. Rev. Lett. 93 (2004) 156801.
[49] H.L. Xin, A. Holewinski, N. Schweitzer, E. Nikolla, S. Linic, Top. Catal. 55 (2012) 376.
[50] A. Nilsson, L.G.M. Pettersson, B. Hammer, T. Bligaard, C.H. Christensen, J.K. Norskov, Catal. Lett. 100 (2005) 111.
[51] F. Abild-Pedersen, J. Greeley, J. Nørskov, Catal. Lett. 105 (2005) 9.
[52] M. Mavrikakis, B. Hammer, J.K. Nørskov, Phys. Rev. Lett. 81 (1998) 2819.
[53] J.L. Zhang, M.B. Vukmirovic, Y. Xu, M. Mavrikakis, R.R. Adzic, Angew. Chem. Int. Ed. 44 (2005) 2132.
[54] J.K. Nørskov, F. Abild-Pedersen, F. Studt, T. Bligaard, PNAS 108 (2011) 937.